

Characterization of analog modulation of AlGaAs lasers and the induced intensity noise

Moustafa AHMED^{1,2}, Nour Zaki EL-SAYED², Hameeda IBRAHIM² and Kamal ABDELHADY²

¹*Department of Physics, Faculty of Science, King Abdelaziz University, 80203 Jeddah-SAUDI ARABIA*

²*Department of Physics, Faculty of Science, Minia University, 61519 El-Minia-EGYPT
e-mail: mostafa.hafez@science.miniauniv.edu.eg*

Received: 13.03.2011

Abstract

The dynamics of AlGaAs laser diodes under analog intensity modulation are characterized and the associated intensity noise is evaluated. The study is based on numerical solution of the stochastic rate equations of semiconductor lasers. Based on the shape of the modulated laser signal, the modulation dynamics are classified into eight distinct types. Four types are characterized by continuous periodic signals, and three types have periodic pulsing signals. These signals happen to have period doubling or superposed by sub-peaks from the relaxation oscillations of the laser. The last type is chaos, in which the signal is irregular and non-uniform. The noise results show that the relative intensity noise is closest to the quantum level under weak modulation where the laser signal is sinusoidal. LF-RIN is pronounced when the laser emits irregular spike-like pulses under low-frequency strong modulation. The chaotic dynamics dominate the region of strong with modulation frequencies around the relaxation frequency of the laser.

Key Words: Analog modulation, modeing and simulation, noise, semiconductor laser

1. Introduction

Semiconductor lasers are used in many applications, including systems for optical fiber communications and common items such as optical disc readers (CD and DVD). In the latter systems, AlGaAs lasers are commonly used for reading from and writing to the optical disc. Due to optical feedback from the reflecting disc surface into the laser cavity, the noise level of the laser may be enhanced, causing errors in the reading/writing process [1]. A common technique to reduce this optical feedback noise is to modulate the laser signal with a weak sinusoidal signal with frequencies close to the resonance frequency of the laser cavity [2, 3]. Under this high speed modulation and when the amplitude of the modulating signal is large, one can obtain short (picoseconds) optical pulses [4, 5] for use in time resolved dynamical studies and for carrying information at high bit rates in optical communication systems [6, 7]. This high speed modulation is affected by the nonlinear coupling of the injected charge carriers with the emitted photons in the active layer. This coupling is influenced

by nonlinear gain suppression which originates from the relaxation processes of charge carriers [8]. During the laser transients, this manifests as time delay of the photon emission followed by damped relaxation oscillations [9]. The delay time and relaxation oscillation frequency depend on the current exciting the laser. Depending on the modulation parameters, such nonlinear effects induce inconsistent time variations in the laser signal induced by the electrical excitation. Inconsistencies include irregular periodic signals with relaxation oscillations, induced sub-peaks, period multiplication, or even chaos [10, 11–17].

Ahmed and El-Lafi [9] simulated the modulation dynamics in InGaAsP lasers and their dependence on the modulation parameters. They classified the modulated laser signal into sinusoidal signal (SS), continuous periodic signal (CPS), continuous periodic signal with periodic oscillation (CPSPO), continuous periodic signal with period doubling (CPSPD), periodic pulse (PP), periodic pulse with relaxation oscillation (PPRO) and periodic pulse with period doubling (PPPD) [9]. Later, Ahmed [18] studied the noise content of these types. Since the nonlinear gain in AlGaAs lasers are stronger than that in InGaAsP lasers, this classification of modulation types and their operating conditions are expected to change.

In this paper, we characterize the dynamics of AlGaAs laser diodes under sinusoidal modulation and classify the modulation dynamic types in AlGaAs lasers. The noise content of each type is evaluated and the operating conditions corresponding to lowest noise levels are explored. The study is based on large-signal numerical analysis of the laser rate equations. The results show that the modulation dynamics of AlGaAs lasers are classified into eight types. Four types have regular and uniform signals, namely, SS, CPS and PP. The other five types have irregular signals (with more than one peak); namely, CPSRO, PPRO, CPSPD, PPPD, and chaos. We show that the Relative Intensity Noise (RIN) spectrum coincides with the quantum noise of the unmodulated laser when the laser output is SS. The Low Frequency RIN (LF-RIN) is considerably enhanced and the laser coherency is extremely deteriorated when the laser emits irregular spike-like pulses under low-frequency strong modulation.

This paper is organized as follows. In Section 2, the theoretical model of simulating the laser dynamics and noise under analog modulation is introduced. In Section 3, the numerical calculations, simulation results and discussion are given. Finally, conclusions appear in Section 4.

2. Theoretical model

The analog modulation of semiconductor lasers is described by the following rate equations of the photon number $S(t)$ and injected electron number $N(t)$ for a laser oscillating in a single mode [19]:

$$\frac{dS}{dt} = (G - G_{th})S + C\frac{N}{\tau_e} + F_S(t) \quad (1)$$

$$\frac{dN}{dt} = \frac{1}{e}I(t) - AS - \frac{N}{\tau_e} + F_N(t). \quad (2)$$

Here, G is the optical gain, and is defined in the form [8, 20]

$$G = A - BS, \quad (3)$$

with the coefficients of linear gain A and gain suppression B defined as

$$A = \frac{a\xi}{V}(N - N_g) \quad (4)$$

$$B = B_c (N - N_s), \quad (5)$$

where a being the tangential gain, ξ is the confinement factor of the optical field in the active layer whose volume is V and refractive index and N_g is the electron number at transparency, B_c and N_s are a coefficient and an electron number characterizing B . G_{th} is the threshold gain level of the laser. The last term in equation (1), CN/τ_e , describes the rate of increase of S by spontaneous emission with τ_e being the electron lifetime and C as the spontaneous emission factor. The last terms $F_S(t)$ and $F_N(t)$ in equations (1) and (2) are Langevin noise sources and are added to the equations to describe the intrinsic fluctuations in $S(t)$ and $N(t)$ associated with quantum transitions of electrons between the valence and conduction bands. These noise sources have Gaussian statistics with zero means and are δ -correlated. Techniques of simulating these noise sources using computer random-number generations can be found in reference [21].

The modulation is included in the rate equations in terms of the driving current $I(t)$ which is assumed sinusoidal and given by

$$I(t) = I_b + I_m \cos(2\pi f_m t) \quad (6)$$

where I_b and I_m are the bias and modulation currents, respectively, and f_m as the modulation frequency.

The noise content of the modulated laser signal is measured by the relative intensity noise (RIN), which is evaluated by the following integration over a finite, but long enough, period T :

$$RIN = \frac{1}{\bar{S}^2} \left\{ \frac{1}{T} \left| \int_0^T \delta S(\tau) e^{-j\Omega_r \tau} d\tau \right|^2 \right\}, \quad (7)$$

where $\delta S(t) = S(t) - \bar{S}$ is the fluctuation in $S(t)$ around its time average value \bar{S} and Ω_r is the Fourier circular frequency.

3. Numerical calculations, results and discussion

Rate equations (1) and (2) are solved numerically by the fourth-order Runge-Kutta algorithm [22]. The laser is assumed to be biased above threshold, $I_b = 2I_{th}$, to neglect contributions of the noisy spontaneous emission to the laser output. The corresponding value of $S(t)$ is evaluated via the equation

$$S_b = \frac{I_b - I_{th}}{eG_{th}}, \quad (8)$$

where I_{th} is the threshold current and e is the electron charge. $S(t)$ is evaluated over 512 cycles of period $T_m = 1/f_m$ using an integration step of $\Delta t \sim 5$ ps. The frequency spectrum of RIN of the laser output in equation (7) is calculated by using the fast Fourier transform (FFT) of the calculated values of fluctuations $\delta S(t)$ as [23]

$$RIN = \frac{1}{\bar{S}^2} \frac{\Delta t^2}{T} |FFT[\delta S E(t_i)]|^2. \quad (9)$$

In this calculation, the longer half of the time trajectory of $S(t)$ is considered, which ascertains that the transients are discarded and the output is stabilized. FP-AlGaAs lasers emitting at wavelength $\lambda = 780$ nm are considered. Typical values of the parameters of these lasers are listed in the table 1. The corresponding

relaxation oscillation frequency f_r and modulation bandwidth frequency f_{3dB} are determined approximately from the small-signal approach as [24]

$$f_r \approx \frac{1}{2\pi} \sqrt{\left(\frac{a\xi}{V}\right) \left[\frac{a\xi\tau_e}{eV} (I_b - I_g) + B \frac{I_b - I_{th}}{eG_{th}} \right] \frac{I_b - I_{th}}{eG_{th}}} \quad (10)$$

$$f_{3dB} = \frac{1}{2\pi} \sqrt{(\Omega_r^2 - 2\Gamma_r^2) + 2\sqrt{(\Omega_r^2 - \Gamma_r^2)^2 + \Omega_r^2\Gamma_r^2}} \quad (11)$$

with

$$\Gamma_r \approx \frac{1}{2} \left(\frac{a\xi}{V} + B \right) \frac{I_b - I_{th}}{eG_{th}}, \quad (12)$$

where Ω_r and Γ_r are the circular relaxation frequency and damping rate of the laser, respectively. The calculated values are $f_r = 3.6$ GHz and $f_{3dB} = 6.25$ GHz. The modulation results are simulated using the modulation frequency f_m/f_r and modulation index $m = I_m/I_b$ as parameters.

Table 1. List of the parameters of FP-AlGaAs lasers and their typical values used in the calculations.

Symbol	Meaning	Value	Unit
λ	Emission wavelength	780	Nm
a	Tangential gain coefficient	2.75×10^{-12}	$\text{m}^3 \text{s}^{-1}$
ξ	Field confinement factor in the active layer	0.2	—
V	Volume of the active region	150×10^{-18}	m^3
N_g	Electron number at transparency	3.15×10^8	—
C	Spontaneous emission factor	1.023×10^{-5}	—
τ_e	Spontaneous emission lifetime	2.79×10^{-9}	S
N_s	Electron number characterizing gain suppression	2.55×10^8	—
B_c	Coefficient characterizing gain suppression	1.567×10^{-6}	s^{-1}
G_{th}	Threshold gain level	2.823×10^{11}	s^{-1}
I_{th}	Threshold current	22.5	mA

3.1. Deterministic modulation characteristics of semiconductor lasers

First, we elucidate the deterministic dynamics of AlGaAs lasers under analog modulation by dropping the Langevin noise sources from rate equations (1) and (2). Figures 1(a)–(h) plot the eight forms of the modulated laser signal simulated under different modulation conditions. The signal is represented by the time variation of the photon number $S(t)$. The axis of $S(t)$ is normalized by the corresponding bias value S_b , while the time axis is normalized by the period $T_m = 1/f_m$. Figures 1(i)–(p) plots the corresponding ($S(t)$ versus $N(t)$) phase portraits, which are also used to characterize the dynamics types in this paper. The axes are normalized by the corresponding biased values S_b and N_b , respectively. Figure 1(a) characterizes the time variation of the SS type in which the signal is sinusoidal. The figure corresponds to small-signal modulation of $m = 0.1$ with $f_m = 1.6 f_r$. The loop of the (S-N) phase portrait is circular, as shown in Figure 1(i). Figure 1(b) corresponds to weak modulation, $m = 0.4$, with $f_m = 1.6 f_r$, and shows that $S(t)$ varies continuously, uniformly and periodically with time. This type is called CPS (continuous periodic signal). The shown signal is not sinusoidal; it is asymmetric with respect to the average value of the signal. The phase portrait of Figure 1(j) corresponds

to a single (but not circular) loop. This CPS type was observed in AlGaAs lasers in experiments by Henery et al. [11] and predicated in theory by Ahmed and El-Lafi [9].

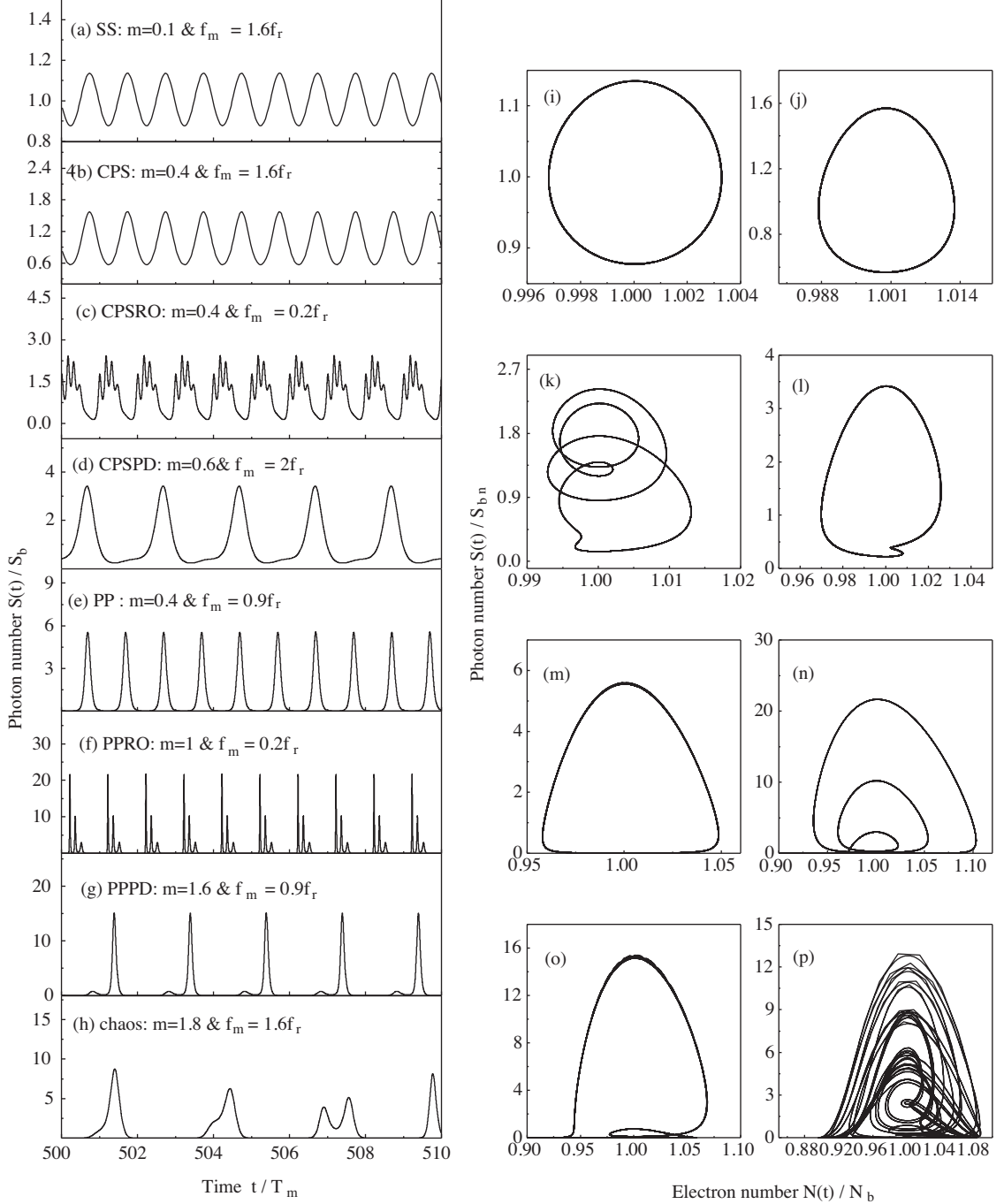


Figure 1. Typical characteristics of (a) SS ($m = 0.1$ and $f_m = 1.6f_r$), (b) CPS ($m = 0.4$ and $f_m = 1.6f_r$), (c) CPSRO ($m = 0.4$ and $f_m = 0.2f_r$), (d) CPSPD ($m = 0.6$ and $f_m = 2.0f_r$), (e) PP ($m = 0.4$ and $f_m = 0.9f_r$), (f) PPRO ($m = 1.0$ and $f_m = 0.2f_r$), (g) PPPD ($m = 1.6$ and $f_m = 0.9f_r$), and (h) chaos ($m = 1.8$ and $f_m = 1.6f_r$). Plots (i)–(p) are the corresponding (S-N) phase portraits.

Figure 1(c) characterizes the CPSRO type, which is another type of CPS but the periodic cycles are superposed by sub-peaks. The figure corresponds to $m = 0.4$ and $f_m = 0.2f_r$. The shown four superposing peaks stem from relaxation oscillations and were observed in AlGaAs lasers by Henry et al. [11] and predicted in theory by Ahmed and El-Lafi [9]. It can be understood as follows. The relatively large value of m means that the valleys of the current $I(t)$ become close to the threshold level I_{th} , which causes also drop of the valleys of gain $G(t)$ close to G_{th} . Because $f_m = 0.3f_r$, the period T_m is much longer than the setting time of the relaxation oscillations. Therefore, with the instantaneous rise up of $I(t)$, $G(t)$ arises to above threshold and builds up the relaxation oscillations in $S(t)$. The phase portrait plotted in Figure 1(k) indicates a four-loop attractor, which characterizes this type of dynamics and confirms the signal irregularity.

The last investigated type with a continuous time variation is CPSPD in which the signal has one peak in every two successive periods. This type is characterized in Figure 1(d), which is obtained when $m = 0.6$ and $f_m = 2f_r$. The figure shows a typical temporal trajectory of $S(t)$ of this type. The separation of each two successive similar peaks is equal to $2T_m$. The phase portrait of Figure 1(l) has a major loop representing the pronounced peak and a child loop representing the rather weak peak shown in Figure 1(d). This type dominates the region of strong modulation, where $N(t)$ goes far below N_{th} , and frequencies $f_m > f_{r0}$. Therefore, the effect of turn-on delay is pronounced in the time variation of $S(t)$ in the form of two unequal peaks.

In other three investigated dynamic types, the laser intensity discontinues in such a way to emit regular and irregular pulses. One type is PP, which is the most preferred type of modulation for semiconductor laser applications in generating short pulses. Figure 1(e) depicts such a type when $m = 0.4$ and $f_m = 0.9f_r$. This strong modulation induces a switching effect from under threshold during the lower cycles of $I(t)$ to above threshold during the upper cycles [9]. The figure shows that $S(t)$ exhibits regular PPs with duration $T_m = 1/f_m$. The effect of gain switching combined with the fact that f_m is comparable to f_r (i.e., T_m is comparable to the setting time of the relaxation oscillations, and there is no chance for the relaxation sub-oscillations to appear) is responsible for pulsation of $S(t)$. When the pulse is too short, this type corresponds to the spike generation predicted by Lee et al. [25].

The phase portrait of Figure 1(m) refers to a single loop; it is much broad around $S(t) \approx 0$ and gets narrower with the increase of $S(t)$.

Figure 1(f) characterizes the PPRO type in which each pulse is periodically superposed with two sub-peaks. This dynamic type is a natural extend of CPSRO with the increase of m . The figure, which is obtained when $m = 1.0$ and $f_m = 0.2f_r$, shows that $S(t)$ exhibits a short and strong pulse followed by two relatively weak sub-peaks in each period T_m .

The irregularity of this type is identified by the phase portrait in Figure 1(n), which shows a triple-loop. The narrower loop refers to the sub-peak.

The PPPD type is illustrated in Figure 1(g) which corresponds to $m = 1.6$ and $f_m = 0.9f_r$. The figure shows that the pulses of $S(t)$ have period doubling. This stronger modulation signifies the effect of the turn-on delay on the time variation of $S(t)$.

The phase portrait of Figure 1(o) shows the double-loop that characterizes this type of pulses with two peaks. These results agree with those reported by Ahmed and El-Lafi [9] in InGaAsP lasers. Also Such period doubling dynamics of AlGaAs lasers were observed in experiments by Chusseau et al. [14] and Henery et al. [11].

In the last investigated type the laser emits pulses for which both the peak values and peak-to-peak interval are irregular, which is a type of chaos.

Typical characteristics of chaos in the time domain are depicted in Figure 1(h), which corresponds to $m = 1.8$ and $f_m = 1.6 f_r$. This strong modulation results in strong switching of the laser from deep under threshold, while the high-speed modulation corresponds to very short modulation period compared with the setting time of the relaxation oscillation. These effects induce high speed and strong gain switching, which results in the shown irregular peak values as well as the peak-to-peak interval.

The chaotic attractor of characterizing this dynamic type is shown in the phase portrait of Figure 1(p).

It is important to investigate influence of the modulation parameters on the investigated types of laser modulation. Of practical interest is to explore the operating regions of the irregular types in order to avoid signal distortion and noise enhancement. For such purposes, the laser dynamics are simulated over wide ranges of the modulation index, $m = 0.1 \rightarrow 2.0$, and modulation frequency, $f_m/f_r = 0.1 \rightarrow 2.0$, using a fine step of 0.1. The modulation parameters, m and f_m , corresponding to each of the investigated eight types of modulation dynamics are mapped in the (m versus f_m) diagram of Figure (2). Each region in the diagram then corresponds to one of the seven modulation types, enclosing modulation points (m, f_m) that reveal the modulated laser output of such a type.

As shown in Figure 2, the region of the CPS type occupies the region of low values of m over the relevant range of f_m . The range of m in the region of CPS increases with the increase of f_m . Over the lower range of m (small-signal modulation), the CPS approaches sinusoidal signals (SS). It is worth noting that at a given index m of the CPS region, the signal amplitude increases with f_m up to nearly the peak frequency of the response, then decreases with further increase of f_m . Up to $f_m \approx 0.4 f_r$, the further increase of m brings the CPSRO type. For frequencies $0.4 \leq f_m/f_r \leq 0.75$, the increase in m develops the CPS and CPSRO to the PP type, which agrees with the predictions of Kao and Lin [16]. When $f_m = 0.85 f_r$ it was found that the pulse width decreases. The period-doubling dynamics appear when $f_m \leq 0.75 f_r$ and $m \leq 2$. The PPPD type appears first as a transition from the PP type. When $f_m > 1.8 f_r$, the CPSPD type follows the CPS type with the increase of m . The region of chaos dominates the region of high modulation frequencies, $f_m \geq 1.4 f_r$ and very strong modulation, $m \geq 1$; it is an extension of the PPPD type with the increase of m and/or f_m .

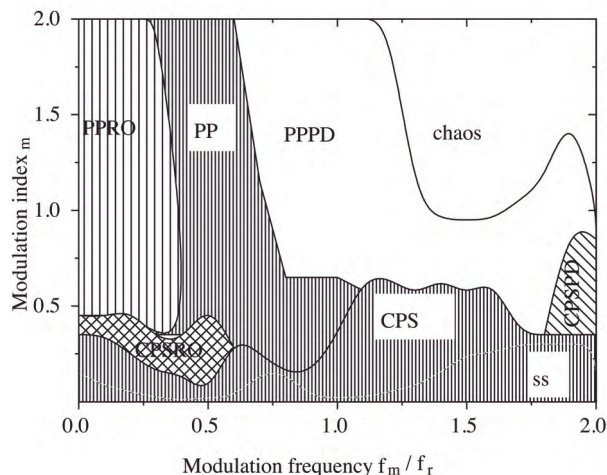


Figure 2. The CPS type dominates the low range of m . Both CPSRO and PPRO appear in the relatively low range of f_m . The period doubling dominates the range of very high m with f_m comparable to or exceeding f_r .

3.2. Noise associated with intensity modulation of semiconductor lasers

In this section, the spectral characteristics of RIN of AlGaAs laser diodes under analog intensity modulation are investigated. Variation of LF-RIN with the modulation parameters is also discussed. These noise properties in each investigated modulation type are compared with those of the unmodulated laser. Figures 3(a)–(h) plot typical frequency spectra of RIN in the eight investigated modulation dynamic types: SS, CPS, CPSRO, CPSPD, PP, PPRO, PPPD and chaos, respectively. The RIN spectrum of the unmodulated laser is plotted also in the figures for comparison. The Fourier frequency axis is normalized by the corresponding modulation frequency f_m of each figure. In Figures 3(c), (f) and (g), the relaxation oscillation peak does not appear due to the low value of f_m compared with f_r .

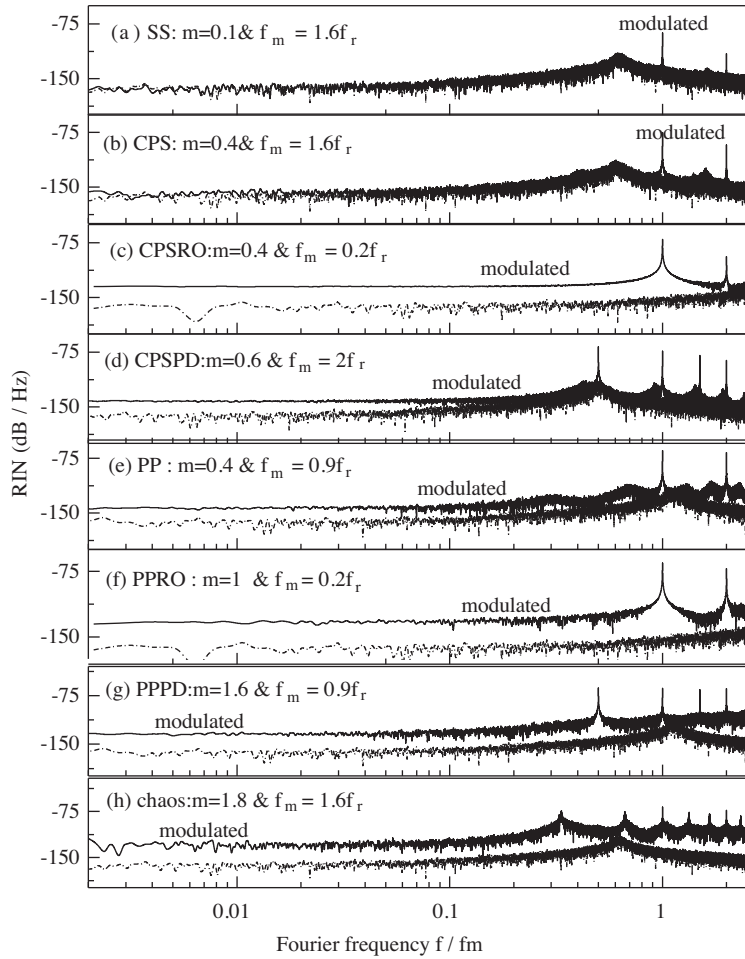


Figure 3. Frequency spectrum of RIN (a) SS ($m = 0.1$ and $f_m = 1.6f_r$), (b) CPS ($m = 0.4$ and $f_m = 1.6f_r$), (c) CPSRO ($m = 0.4$ and $f_m = 0.2f_r$), (d) CPSPD ($m = 0.6$ and $f_m = 2f_r$), (e) PP ($m = 0.4$ and $f_m = 0.9f_r$), (f) PPRO ($m = 1$ and $f_m = 0.2f_r$), (g) PPPD ($m = 1.6$ and $f_m = 0.9f_r$), and (h) chaos ($m = 1.8$ and $f_m = 1.6f_r$).

Figure 3(a) plots a typical frequency spectrum of RIN of the SS type when $m = 0.1$ with $f_m = 1.6f_r$. This RIN spectrum coincides with that of the quantum noise spectrum of the unmodulated laser, except that it has sharp peaks at f_m and its multiples. This coincidence is manifestation of the symmetry, uniformity and

regularity of the sinusoidal signals. Figure 3(b) plots a typical frequency spectrum of RIN of the CPS type when $m = 0.4$ and $f_m = 1.6 f_r$. This RIN spectrum has almost the same levels of that of the unmodulated laser, except that (a) LF-RIN is almost -2 dB/Hz higher and (b) the spectrum has sharp peaks at f_m and its multiples. The small difference of the LF-RIN from that of the unmodulated laser originates from the asymmetry of the CPS. Figure 3(c) characterizes RIN of the CPSRO type when $m = 0.4$ and $f_m = 0.2 f_r$. The figure shows that the RIN spectrum has levels about -20 dB/Hz higher than that of the CPS type with sharp characteristic peaks at f_m and their multiples. LF-RIN is flat with a level of ~ -136 dB/Hz which is higher than those of both the unmodulated laser and CPS type. The last investigated type with a continuous time variation is CPSPD in which the signal has one peak in every two successive periods. This type is characterized in Fig. 1(d), which is obtained when $m = 0.6$ and $f_m = 1.6 f_r$. The low-frequency components are also flat with LF-RIN ~ -142 dB/Hz, which is still higher than that of either the CPS type or the unmodulated laser.

Figure 3(e) characterizes the RIN spectrum of the PP type, which corresponds to $m = 0.4$ and $f_m = 0.9 f_r$. The figure shows that the RIN spectrum is characterized by sharp peaks at f_m and its multiples. Compared with the spectra of the unmodulated laser, the RIN spectrum is almost -20 dB/Hz higher than that of the unmodulated laser. The noise content of the PPRO type is characterized in Figure 3(f), which plots the RIN spectrum when $m = 1$ and $f_m = 0.2 f_r$. The spectrum is characterized by peaks at f_m and its multiples. The RIN spectrum is the worst among the investigated types; the LF-RIN is -132 dB/Hz, which is ~ -20 dB/Hz higher than that of the unmodulated laser. The RIN spectrum of the PPPD type is plotted in Figure 3(g) for $m = 1.6$ and $f_m = 0.9 f_r$. The spectrum is almost -2 dB/Hz lower than that of the PPRO type but is higher than that of the unmodulated laser peaks. This spectrum is characterized by peaks at $f_m/2$ and its higher multiples.

The noise characteristics of the chaotic dynamics are illustrated in Figure 3(h), which plots the RIN spectrum for $m = 1.8$ and $f_m = 1.6 f_r$. The figure shows that the entire RIN spectrum is much higher than that of the unmodulated laser -30 dB/Hz higher. The figure indicates a chaotic spectrum with rather a high peak at $f = f_m$. The peak around f_r is much broader than the other dynamic types.

It is practically important to examine the level of RIN in the low-frequency region, $f_m < 200$ MHz because of its application in the optical disc systems [1]. Variation of the LF-RIN with the modulation index m at frequencies $f_m \ll f_r$, $f_m \sim f_r$ and $f_m \gg f_r$ are plotted in Figures 4(a)–(c) for $f_m = 0.2 f_r$, $f_m = 0.9 f_r$, and $f_m = 1.6 f_r$, respectively. When $f_m = 0.2 f_r$, Figure 4(a) shows that under low-frequency modulation, LF-RIN is lowest under the SS type, when $m \leq 0.1$. The CPS type has higher LF-RIN levels. LF-RIN increases when the CPSRO type is excited and are enhanced when $m > 0.5$ under the PPRO type. LF-RIN is pronounced when $m > 1.4$ under PPRO where the pulse exhibits the first overshoot (spike) of the relaxation oscillations accompanied by smaller discontinuous shots. Furthermore, these relaxation oscillation peaks are unequal, which reflects the irregularity of the PPRO signal. That is, the noise performance of the laser and its coherence are the worst in this regime of modulation. This result was also predicted for InGaAsP lasers by Ahmed [18].

Figure 4(b) shows that when the modulation frequency f_m is comparable to the resonance frequency, $f_m = 0.9 f_r$, LF-RIN is higher under the PP type than under both the SS and CPS types. In the region of the PP type, LF-RIN increases with the increase of m due to the increase of the degree of irregularity. The PPPD is associated with LF-RIN levels ~ -132 dB/Hz, which is almost equal to that of the most irregular operation of the PP type. It is clear in Figure 4(c) of the high-speed modulation, $f_m = 1.6 f_r$, that the LF-RIN level in the regime of PPPD is higher than that in the regime of the SS and CPS. The LF-RIN level increases more

reaching -125 dB/Hz when chaos is induced in the region of strong modulation, $m > 1$. It is worth noting that the LF-RIN level in the CPS region is much lower than its level when $f_m = 0.1 f_r$ or $0.9 f_r$.

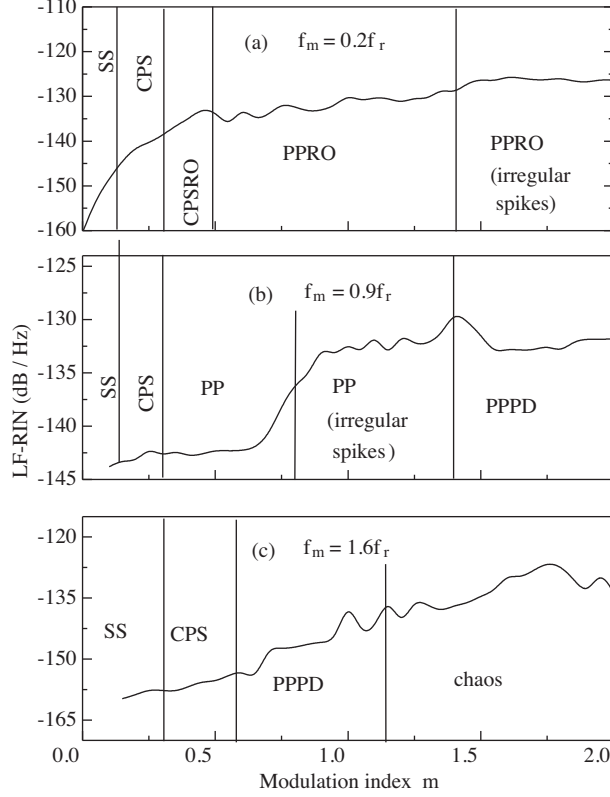


Figure 4. Variation of LF-RIN with modulation index m under (a) low frequency $f_m = 0.2 f_r$ modulation, (b) low frequency modulation $f_m = 0.9 f_r$ and (c) high frequency modulation $f_m = 1.6 f_r$. The LF noises are most enhanced under the chaos type.

4. Conclusions

The dynamics of AlGaAs laser diodes and the associated RIN were investigated under analog intensity modulation. The laser signal is CPS, CPSRO, CPSPD, PP, PPDRO, PPPD or chaotic under modulation. Basing on the obtained results, the following conclusions can be traced.

1. The SS and CPS types occupy the region of low values of m over the relevant range of f_m . Up to $f_m \approx 0.4 f_r$, further increase of m brings the CPSRO type. For frequencies $0.4 \leq f_m / f_r \leq 0.75$, the increase in m develops the CPS and CPSRO to the PP type. The period-doubling dynamics appear when $f_m \leq 0.75 f_r$ and $m \leq 2$. The PPPD type appears first as a transition from the PP type. When $f_m > 1.8 f_r$, the CPSPD type follows the CPS type with the increase of m . The region of chaos dominates the region of high modulation frequencies, $f_m \geq 1.4 f_r$ and very strong modulation, $m \geq 1$ as extension of the PPPD type.
2. When $f_m \ll f_r$, LF-RIN is lowest under the SS type. It increases when the CPSRO type is excited and

are enhanced under the PPRO type. LF-RIN and is pronounced when the pulse exhibits the first overshoot (spike) of the relaxation oscillations accompanied by smaller discontinuous shots.

3. When $f_m \sim f_r$, LF-RIN is higher under the PP type than under the SS and CPS types. In the region of the PP type, LF-RIN increases with the increase of m due to the increase of the degree of irregularity. The PPPD is associated with LF-RIN levels ~ -132 dB/Hz, which is almost equal to that of the most irregular operation of the PP type.
4. When $f_m \gg f_r$, the LF-RIN level in the regime of PPPD are higher than those in the regime of the CPS and SS. The LF-RIN level increases more reaching -125 dB/Hz when chaos is induced in the region of strong modulation, $m > 1$. It is worth noting that the LF-RIN level in the CPS region is much lower than its level when $f_m = 0.1$ or $0.9 f_r$.

References

- [1] G. P. Agrawal and N. K. Dutta, *Semiconductor lasers*, 2nd ed, vol. 1 (Van Nostrand Reinhold, New York, 1993) p. 255.
- [2] M. Yamada and T. Higashi, *IEEE J Quantum Electron.*, **27**, (1991), 380.
- [3] A. T. Ryan, G. P. Agrawal, G. R. Gray and E. C. Gage, *IEEE J Quantum Electron.*, **30**, (1994), 668.
- [4] D. Bimberg, K. Ketterer, H. E. Scholl and H. P. Vollmer, *Electron Lett.*, **20**, (1984), 343.
- [5] R. Stevens, MSc Thesis, University College, Ireland, 1996.
- [6] O. N. Makeyev, Y. A. Zarkevitch and V. I. Smirnov, *Telecom Radio Eng*, **45**, (1990), 41.
- [7] G. C. Brooks, *Telecom J.*, **58**, (1988), 88.
- [8] M. Yamada, Y. Suematsu. *J. Appl. Phys.*, **52**, (1981), 2653.
- [9] M. Ahmed, El-Lafi A, *laser technology*, **40**, (2008) 809.
- [10] G. P. Agrawal, *Appl. Phys. Lett.*, **49**, (1986), 1013.
- [11] E. Henery, L. Chusseau and J. M. Lourtioz, *IEEE J. Quantum Electron.*, **26**, (1990), 633.
- [12] M. Tang and S. Wang, *Appl. Phys. Lett.*, **50**, (1987), 1861.
- [13] Y. Hori, H. Serizawa and H. Sato, *J. Opt. Soc. Am. B*, **5**, (1988), 1128.
- [14] L. Chusseau, E. Henery and J. M., *Appl. Phys. Lett.*, **55**, (1989), 822.
- [15] Y. H. Kao and C. H. Tsai, *Rev. Sci. Inst.*, **63**, (1992), 75.
- [16] Y. H. Kao and H. T. Lin, *Phys Rev A*, **48**, (1993), 2292.
- [17] M. Tang, S. Wang, *Appl. Phys. Lett.*, **48**, (1986), 900.
- [18] M. Ahmed, *J. Appl. Phys*, **41**, (2008), 1.

- [19] M. Ahmed, M. Yamada and S. Mahmoud, *J. Appl. Phys.*, **101**, (2007), 3119.
- [20] M. Ahmed, *Int. J. Num. Model.*, **17**, (2004), 147.
- [21] M. Ahmed and M. Yamada, *J. Appl. Phys.*, **84**, (1998), 3004.
- [22] R. L. Burden, J. D. Faires, and A. C. Reynolds, Numerical analysis. 2nd ed, vol. 2, (Weber and Schmidt, Boston. 1981).
- [23] M. Ahmed, M. Yamada, and M. Saito, *IEEE J. Quantum Electron.*, **37**, (2001), 1600.
- [24] A. EL-Lafi. MSc Thesis, Academy of Graduate Studies, Libya, 2007.
- [25] C. H. Lee, T. H. Yoon and S. Y. Shin, *Appl. Phys. Lett.*, **46**, (1984), 95.